Biomechanics of Traumatic Brain Injury: Influences of the Morphologic Heterogeneities of the Cerebral Cortex

R.J.H. Cloots, H.M.T. Gervaise, J.A.W. van Dommelen, and M.G.D. Geers

Materials Technology Institute, Eindhoven University of Technology, P.O. Box 513, 5600 MB Eindhoven, The Netherlands

Abstract—Traumatic brain injury (TBI) can be caused by accidents and often leads to permanent health issues or even death. Brain injury criteria are used for assessing the probability of TBI, if a certain mechanical load is applied. The currently used injury criteria in the automotive industry are based on global head kinematics. New methods, based on finite element modeling, use brain injury criteria at lower scale levels, e.g., tissue-based injury criteria. However, most current computational head models lack the anatomical details of the cerebrum. To investigate the influence of the morphologic heterogeneities of the cerebral cortex, a numerical model of a representative part of the cerebral cortex with a detailed geometry has been developed. Several different geometries containing gyri and sulci have been developed for this model. Also, a homogeneous geometry has been made to analyze the relative importance of the heterogeneities. The loading conditions are based on a computational head model simulation. The results of this model indicate that the heterogeneities have an influence on the equivalent stress. The maximum equivalent stress in the heterogeneous models is increased by a factor of about 1.3–1.9 with respect to the homogeneous model, whereas the mean equivalent stress is increased by at most 10%. This implies that tissue-based injury criteria may not be accurately applied to most computational head models used nowadays, which do not account for sulci and gyri.

Keywords—Traumatic brain injury, Brain tissue, Cerebrum, Cerebral cortex, Inhomogeneities, Finite element model.

INTRODUCTION

The brain is often one of the most seriously injured parts of the human body in case of a road traffic crash situation.[1,21,41] The incidence rate and mortality rate in Europe are estimated to be 235 and 15.4 per 100,000 of the population per year, respectively.[41] Traumatic brain injury (TBI) is therefore considered as a widespread problem. Understanding the mechanisms inducing TBI is necessary for reducing the number of occurrences, e.g., by developing more appropriate protective systems and diagnostic tools.

Brain injury criteria are used for the assessment of the probability of TBI for certain mechanical loading conditions. The most commonly used injury criterion in the automotive industry is the Head Injury Criterion (HIC).[16,43] It is developed to predict TBI resulting from a translational acceleration of the head. One of the drawbacks of the HIC is that it is based on global kinematic data to predict TBI, whereas actual brain damage is caused at the cellular level as a consequence of tissue strains and stresses.[35] Furthermore, it is based on experimental data, in which only anterior–posterior contact loading has been applied to human cadavers, not accounting for angular accelerations of the head. For a better approximation of the relation between TBI and a mechanical load, more advanced methods have been developed. For instance, three-dimensional finite element (FE) head models have been developed to predict brain injury.[2,6,7,9,17,22,38,42,45,47] With these numerical head models, different injury mechanisms and loading conditions can be distinguished. However, in these models, the heterogeneous anatomy of the cerebrum is usually represented by a relatively homogeneous geometry. A comparison between the homogeneous geometry of a typical finite element head model and the complex structure of a real brain is given in Fig. 1. The main function of the heterogeneous morphology is to increase the cortical surface in order to obtain a more complex level of the brain functions.[34] The most recent numerical head models include ventricles and the invaginations of the dura mater, but none include the convolutions of the cerebral cortex. Consequently, the stresses and strains that are predicted from these models likely do not represent actual tissue stresses and strains, at least in the cortex. Therefore, although tissue-based injury criteria may be used, their accuracy is expected to be limited. This might prohibit the direct use of tissue-based injury
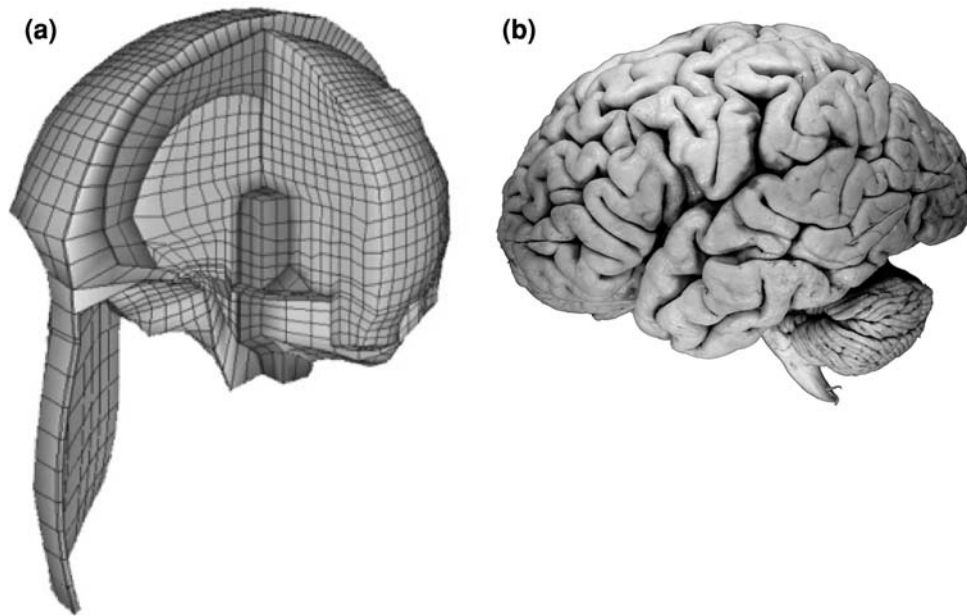
FIGURE 1. (a) Numerical head model developed by Claessens.[6,7] (b) Lateral view of the human brain. Adapted from Welker et al.[44]

criteria. Such criteria predict injury at the tissue level and are based on *in vitro* and *in vivo* experiments.[3,4,10,11,13,31,32] For a direct application of tissue-based injury criteria in a computational head model, a more detailed description of the biomechanical behavior of the cerebrum may be required, which can be achieved by including its morphologic heterogeneities in these models. A few two-dimensional FE models of the brain containing the convolutions of the cerebral cortex have been described in literature. Miller *et al.*[30] compared different modeling techniques for the relative motion between the brain and the cranium. Nishimoto and Murakami[33] developed a model to investigate the relation between brain injury and the HIC. However, these models have not been developed with the purpose of investigating the local biomechanics at the level of these convolutions. No conclusions have been drawn from these studies on the biomechanical influence of the heterogeneities of the cerebral cortex, due to the limited spatial resolution of the mesh.

Physical experiments have been conducted in several studies to investigate the biomechanical consequences of the heterogeneities of the cerebrum.[14] In a study by Bradshaw *et al.*,[5] a gel-filled chamber that represented the brain and skull in a coronal plane including the falx cerebri and the sulci of the cerebral cortex was subjected to a rotation with a peak acceleration of approximately 7800 rad s^{-2}. An increase of the maximum principle strain in the cerebral cortex due to the sulci was found.

The aim of this study is to investigate the biomechanical influences of the morphologic heterogeneities in the cerebral cortex. To achieve this, several two-dimensional FE models with detailed geometries of a part of the cerebral cortex have been developed. Also, an FE model with a homogeneous morphology of the cortex has been made. The loading conditions are based on simulations with a computational head model as used by Brands *et al.*[6] The results of the simulations of the heterogeneous models will be compared to those of the homogeneous model.

METHODS

In this study, plane strain models of small sections of the cerebrum are made using the FE code Abaqus 6.6-1 (HKS, Providence, USA). An explicit time integration is used, anticipating a dynamic load with a high magnitude and a short duration. The time increments are limited by the stability condition, which is determined in the global estimator function in Abaqus.

Geometries

To investigate the influence of the heterogeneities of the cerebral cortex, a homogeneous model and three heterogeneous models have been developed. The heterogeneous models, which are shown in Figs. 2a, 2c, and 2d have detailed geometries of a small part of the cerebrum, including also a part of the cerebrospinal fluid
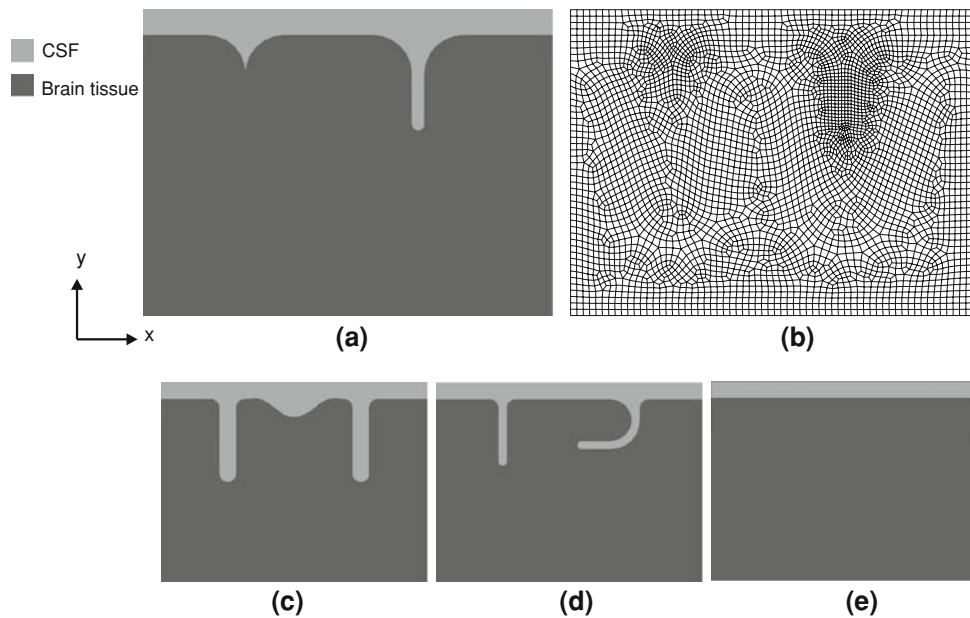
FIGURE 2. (a) Heterogeneous geometry 1 and (b) its spatial discretization. (c) Heterogeneous geometry 2. (d) Heterogeneous geometry 3. (e) Homogeneous geometry.

(CSF). The cranium is modeled by a boundary constraint, as will be detailed further on. Since the dura mater and the arachnoid are connected to the inside of the cranium in the region that is modeled,[29,34] it is assumed that they can be ignored for this situation. The pia mater, which is a thin and delicate membrane covering the brain,[29,34] is also not included, since it is expected to have no mechanical influence for the used loading conditions. The same assumption is used for the arachnoid trabeculae, which extend from the arachnoid to the pia mater and are less existent inside the sulci.[34]

The first geometry has one narrow sulcus on the right hand side and a small part of a sulcus on the left hand side. The second geometry contains two deeper and wider sulci than the other two geometries. The third geometry consists of one vertical sulcus and one partly horizontal sulcus, where horizontal and vertical refer to the x- and y-direction, respectively. These geometries, which represent typical stylized shapes of the cerebral cortex, are based on the topological studies by Mai et al.[27] The left and right boundaries of the models are chosen to be periodic, i.e., the internal geometries near the opposite boundaries match. The periodicity of the boundary conditions will be explained further on. The models do not distinguish between gray (cerebral cortex) and white matter. In Fig. 2e, the homogeneous model is shown. Similar to the heterogeneous models, it also consists of CSF and brain tissue, but it does not contain any gyri and sulci. The outer dimensions of each model are 32 mm by 24 mm. The meshes consist of bi-linear, quadrilateral, reduced integration elements with hourglass control.

The heterogeneous models also contain a small number of triangular elements. The total number of elements of the heterogeneous models ranges from 4243 to 4533 elements. The homogeneous geometry consists of 3072 elements.

Material Properties

For the material properties of the CSF, a nearly incompressible, low shear modulus elastic solid has been assumed, since the shear stress in the brain tissue due to the applied loading conditions is estimated to be about a factor 10^4 higher than that in the CSF. The material properties are listed in Table 1. The shear modulus of CSF is estimated from the loading conditions that are described further on by using $G = \eta\dot{\gamma}/\gamma$, in which G is the elastic shear modulus, η is the viscosity, γ is the estimated shear strain, and $\dot{\gamma}$ is the estimated shear rate. Because two different loading conditions have been used, also two different estimates for the CSF shear modulus have been used. However, with these shear moduli being much lower than that of the brain tissue, the exact values of these estimates do not affect the outcome of this study. The bulk modulus is obtained from literature.[2,47]

The material properties of the brain tissue are described by a non-linear viscoelastic constitutive model that has been developed by Hrapko et al.[19] This model was found to accurately describe the response of brain tissue for large deformations in both shear and compression. This model is extended here to account for compressibility.

TABLE 1.   Linear material parameters.

	Bulk modulus (GPa)	Shear modulus (Pa)	Time constant (s)
CSF	2.2	0.036[a]	∞
		0.12[b]	∞
Brain tissue	2.5	182.9	∞
		9884	0.00013
		835.5	0.012
		231.2	0.35
		67.1	4.62
		3.61	12.1
		2.79	54.3

[a]Shear modulus in case of loading condition A.
[b]Shear modulus in case of loading condition B.

The constitutive model consists of an elastic part, denoted by the subscript 'e', and a (deviatoric) viscoelastic part, denoted by the subscript 've', with N viscoelastic modes. The total Cauchy stress tensor $\boldsymbol{\sigma}$ is written as

$$\boldsymbol{\sigma} = \boldsymbol{\sigma}_e^h + \boldsymbol{\sigma}_e^d + \sum_{i=1}^{N} \boldsymbol{\sigma}_{ve_i}^d \tag{1}$$

in which the superscripts 'h' and 'd' denote the hydrostatic and the deviatoric part, respectively. For simplicity, the subscript i indicating the number of the viscoelastic mode will be omitted from this point on. The hydrostatic part of Eq. (1) is defined as

$$\boldsymbol{\sigma}_e^h = K(J-1)\boldsymbol{I} \tag{2}$$

where K is the bulk modulus and $J = \det(\boldsymbol{F})$ is the volume change ratio.

The deviatoric elastic mode describes a non-linear response to the deformation gradient tensor $\boldsymbol{F}$, which is given by

$$\boldsymbol{\sigma}_e^d = \frac{G_\infty}{J}\left[(1-A)\exp\left(-C\sqrt{b\tilde{I}_1 + (1-b)\tilde{I}_2 - 3}\right) + A\right] \left[b\tilde{\boldsymbol{B}}^d - (1-b)(\tilde{\boldsymbol{B}}^{-1})^d\right] \tag{3}$$

where G_∞ is the elastic shear modulus, $\tilde{\boldsymbol{B}} = J^{-\frac{2}{3}}\boldsymbol{B}$ is the isochoric part of the Finger tensor $\boldsymbol{B}$, and $\tilde{I}_1$ and $\tilde{I}_2$ are the first and second invariant of the isochoric Finger tensor $\tilde{\boldsymbol{B}}$, respectively. A, C, and b are fitting parameters describing the non-linearity of the elastic response.

The third term on the right hand side of Eq. (1) consists of the summation of the viscoelastic modes. The deformation gradient tensor $\boldsymbol{F}$ is partitioned into an elastic deformation gradient tensor $\boldsymbol{F}_e$ and a viscous deformation gradient tensor $\boldsymbol{F}_v$ by assuming multiplicative decomposition[25,36]:

$$\boldsymbol{F} = \boldsymbol{F}_e \cdot \boldsymbol{F}_v \tag{4}$$

The decomposition involves a fictitious intermediate state, which could exist after application of merely the viscous deformation gradient tensor $\boldsymbol{F}_v$. This is the stress-free state, which after application of the elastic deformation tensor $\boldsymbol{F}_e$ transforms into the final state. The third term on the right hand side of Eq. (1) describes the viscoelastic contribution to the stress as follows:

$$\boldsymbol{\sigma}_{ve}^d = \frac{G}{J}\left[a\tilde{\boldsymbol{B}}_e^d - (1-a)(\tilde{\boldsymbol{B}}_e^{-1})^d\right] \tag{5}$$

with G the shear modulus, $\tilde{\boldsymbol{B}}_e = J^{-\frac{2}{3}}\boldsymbol{B}_e$ the isochoric part of the elastic Finger tensor $\boldsymbol{B}_e$, and a a fitting parameter.

The viscous deformation $\boldsymbol{F}_v$ is assumed to be volume-invariant, i.e., $\det(\boldsymbol{F}_v) = 1$ and $J_e = \det(\boldsymbol{F}_e) = J$. The viscous rate of deformation tensor is calculated from the flow rule as

$$\boldsymbol{D}_v = \frac{\boldsymbol{\sigma}_{ve}^d}{2\eta(\tau)} \tag{6}$$

where the dynamic viscosity η is a function of the scalar equivalent stress measure $\tau = \sqrt{\frac{1}{2}\boldsymbol{\sigma}^d : \boldsymbol{\sigma}^d}$, for which the Ellis model is adopted:

$$\eta(\tau) = \eta_\infty + \frac{\eta_0 - \eta_\infty}{1 + \left(\frac{\tau}{\tau_0}\right)^{(n-1)}} \tag{7}$$

with subscripts 0 and ∞ denoting the initial and infinite values, respectively. The initial value for the viscosity is defined as $\eta_0 = G\lambda$, whereas the infinite viscosity is defined as $\eta_\infty = k\eta_0$. Here, λ refers to the time constant.

Although differences between the material properties of the gray and white matter may exist, these differences are not well characterized. Therefore, no distinction between gray and white matter has been made in this study, except for the investigation of the influence of varying the material properties of gray matter with respect to those of white matter (see the Discussion and Conclusions). For simulating a head impact situation representative of road traffic accidents, an extra viscoelastic mode with a smaller time constant has been added to the behavior as characterized by Hrapko *et al.*[19] The extra mode[18] is based on the experimental data from Hrapko and co-workers in combination with the data by Shen *et al.*[39] The linear material properties are listed in Table 1. The values of the non-linear viscoelastic parameters are shown in Table 2.

TABLE 2.   Non-linear material parameters for brain tissue.

Elastic	Viscous
$A = 0.73$	$\tau_0 = 9.7$ Pa
$C = 15.6$	$n = 1.65$
$a = 1$	$k = 0.39$
$b = 1$	

Boundary Conditions

The boundary conditions have been chosen such that they represent the biomechanical influences of the surroundings on the cerebral cortex model. Figure 3 shows the labeling of the corner nodes and the boundaries. The symbols x and y denote the components of position vector $\vec{x}$ with respect to a Cartesian vector basis $(\vec{e}_x, \vec{e}_y)$, whereas u and v are the components of the displacement vector $\vec{u}$ with respect to this basis.

The Young's modulus of the cranium is much higher than that of brain tissue.[19,46] Still, in a contact loading situation of the head the deformation of the skull is important, because it initiates strain waves in the brain tissue. In this study, however, only inertial loading of the head is considered and therefore the cranium is assumed to be rigid. The cranium is incorporated in the boundary condition at Γ_3. Because of the low shear modulus of the CSF, the influence of the rigid constraint associated with the cranium at boundary Γ_3 in the x-direction can be neglected. Provided no rotation of the model occurs, the constraint equation for all nodes on boundary Γ_3 is

$$v|_{\Gamma_3} = v_s \qquad (8)$$
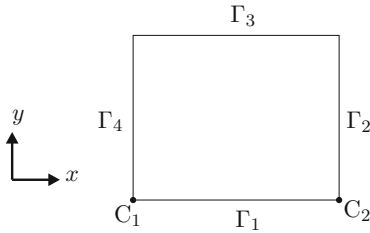
with v_s the vertical displacement of the skull.

FIGURE 3. Labeling of corner nodes and boundaries.

The boundaries Γ_2 and Γ_4 are subjected to periodic boundary conditions[23]:

$$\vec{u}|_{\Gamma_2} - \vec{u}|_{\Gamma_4} = \vec{u}|_{C_2} - \vec{u}|_{C_1} \qquad (9)$$

These constraints imply that throughout the deformation process the shapes of the opposite boundaries, Γ_2 and Γ_4, remain identical to each other, while the tractions on opposite boundaries are opposite to satisfy stress continuity, which can be written as

$$\boldsymbol{\sigma} \cdot \vec{n}_2 = -\boldsymbol{\sigma} \cdot \vec{n}_4 \qquad (10)$$

with $\boldsymbol{\sigma}$ the Cauchy stress tensor and $\vec{n}_i$ the unit outward normal vector of boundary Γ_i.

The lower boundary, Γ_1, of the brain tissue in the model lies adjacent to brain tissue in neighboring regions. Therefore, boundary Γ_1 has to be constrained accordingly. The applied constraint on Γ_1 is obtained by tying all nodal displacements on Γ_1 to a linear interpolation between the displacements of corner nodes C_1 and C_2. For any node on boundary Γ_1, this results in

$$\vec{u}|_{\Gamma_1} = \vec{u}|_{C_1} + \frac{||\vec{x}_0|_{\Gamma_1} - \vec{x}_0|_{C_1}||}{||\vec{x}_0|_{C_2} - \vec{x}_0|_{C_1}||} \left(\vec{u}|_{C_2} - \vec{u}|_{C_1} \right) \qquad (11)$$

with the subscript 0 denoting the initial configuration. The displacements of corner nodes C_1 and C_2 are prescribed and calculated from the applied loading conditions.

The loading conditions of the cerebral cortex model (micro-level in Fig. 4) are based on the loading conditions that have been used by Brands *et al.*[6] for a three-dimensional numerical head model (macro-level in Fig. 4). In that model, an eccentric rotation has been applied to the skull to simulate an angular head acceleration around the neck-shoulder joint in the
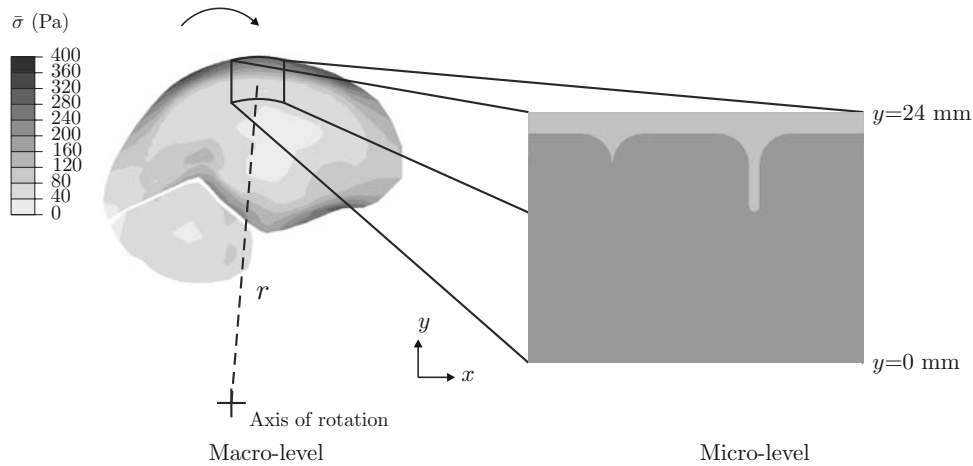

FIGURE 4. The loading conditions of the cerebral cortex model (micro-level) are derived from the region of interest in a parasagittal cross-section (15 mm offset from the midsagittal plane) of the head model (macro-level). Shown at the macro-level is the equivalent stress field of the head model at 10 ms.

sagittal plane in the anterior–posterior direction. The eccentricity has been chosen to represent a typical neck length. The axis of rotation has been positioned at 155 mm below the anatomical origin, i.e., the ear hole projected to the sagittal plane. The rotation of the head model consists of two successive sine functions that describe the angular acceleration:

$$0\,\text{s} < t \leq 0.010\,\text{s} : \dot{\omega}(t) = 250\pi \sin(100\pi t) \qquad (12)$$

$$0.010\,\text{s} < t \leq 0.030\,\text{s} : \dot{\omega}(t) = -125\pi \sin(50\pi(t - 0.010)) \qquad (13)$$

In Eqs. (12) and (13), the angular acceleration $\dot{\omega}$ is given in rad s^{-2}.

The loading conditions are applied to the cerebral cortex model by means of body forces. In all integration points of the elements in the model, a non-uniform body force is imposed that reversely simulates the inertial forces:

$$\vec{q}(\vec{x}, t) = \rho(\vec{x})\ddot{u}(y, t)\vec{e}_x \qquad (14)$$

in which $\vec{q}$ represents the distributed load per unit of volume, ρ is mass density, t is time, and $\ddot{u}$ refers to the acceleration in the x-direction that is represented by these body forces. Note that for the head model the loading conditions contain an angular component, whereas the cerebral cortex model uses translational loading conditions. Because only a small part of the head is modeled and because of the small rotation of the head model with a maximum of 4°, the loading of the cerebral cortex model is assumed to be translational in x-direction only.

The loading conditions of the cerebral cortex model, i.e., the representative accelerations $\ddot{u}(y, t)$, are calculated from the head model (from the region indicated in Fig. 4) in two different approaches:

A. In the first approach, the input accelerations of the head model are used to define the loading condition of the cerebral cortex model. This approach will be referred to as loading condition A.

The translational acceleration $\ddot{u}$ can be calculated using

$$\ddot{u}(y, t) = \dot{\omega}(t)\, r(y) \qquad (15)$$

with $\dot{\omega}$ the angular acceleration, which is defined by Eqs. (12) and (13), and r the radius from the axis of rotation (neck-shoulder) in the head model to a point in the region of interest. The radius r is a function of the y-position in the cerebral cortex model. It varies between $r(0) = 0.251$ m at boundary Γ_1 to $r(0.024) = 0.275$ m at Γ_3. The accelerations $\ddot{u}$ at Γ_1 and Γ_3 are depicted in Fig. 5a. All other accelerations are interpolated linearly between these two boundaries, thereby creating a gradient across the height of the model. The acceleration gradient is important for the resulting shear stresses. Figure 5b shows the acceleration profile of the cerebral cortex model. The accelerations are used to calculate the body forces as a function of both time and y-position.

The disadvantage of this loading condition is that a spatially constant acceleration gradient is assumed and therefore it does not account for the influence of the geometry of the cranium. To account for the geometry of the head, another loading condition has been developed that is described next.

B. The second approach, loading condition B, uses output accelerations from a global head model simulation as the input of the cerebral cortex model. For this, a modified version of the head model, as used by Brands et al.,[6] has been employed in the simulation code Madymo, in which the constitutive model for brain tissue by Hrapko et al.[19] has been implemented. The accelerations obtained from the region inside the box in Fig. 4 from the head model are imposed on the cerebral cortex model. Hence, the influence of the geometry of the head is modeled indirectly by means of an acceleration profile that is obtained from the head model.

The displacements of the brain tissue in the head model in the field of interest are almost entirely in
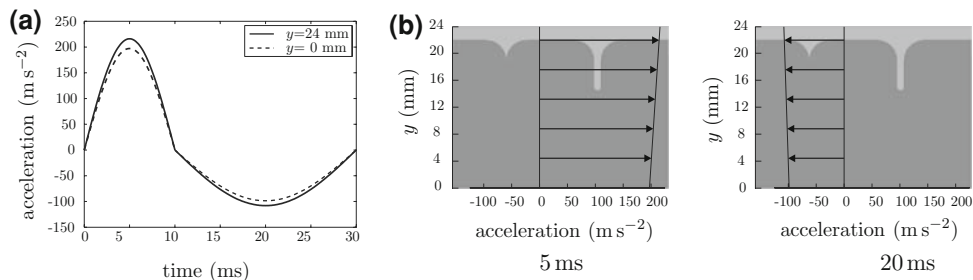

FIGURE 5. Loading condition A. (a) Acceleration at the upper and lower boundary of the cerebral cortex model. (b) Acceleration profiles at different times.
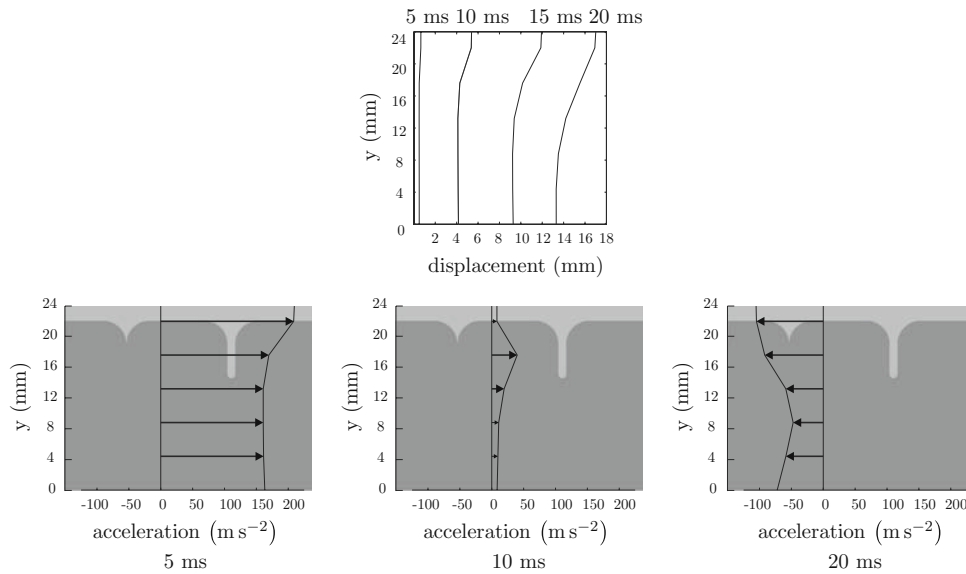
FIGURE 6. Loading condition B: displacement (top) and acceleration (bottom) profiles derived from the output of the head model.

the x-direction justifying the assumption of inertial loading (of the cerebral cortex model) in the x-direction only. In Fig. 6, the acceleration profiles as a function of the y-position are shown at 5, 10, and 20 ms. Similar to loading condition A, the accelerations are used to calculate the body forces as a function of both time and y-position.

In order to quantify the influence of the morphologic heterogeneities, the equivalent stress $\bar{\sigma} = \sqrt{\frac{3}{2}\boldsymbol{\sigma}^{\mathrm{d}} : \boldsymbol{\sigma}^{\mathrm{d}}}$ is used, in which $\boldsymbol{\sigma}^{\mathrm{d}}$ is the deviatoric part of the Cauchy stress tensor $\boldsymbol{\sigma}$. The equivalent stress is chosen, because the simulations are based on an angular acceleration of the head, in which deviatoric stresses are considered to be the most important.[30] The maximum principal strain is considered important as well with respect to diffuse axonal brain injury.[3,30] Therefore, also the maximum principal logarithmic strain is used to quantify the influence of the morphologic heterogeneities.

RESULTS

Figure 7 depicts the development in time of the equivalent stress fields for the homogeneous model (top row) and the heterogeneous models from the simulation with loading condition A. Stress concentrations are present in the heterogeneous models at the surface of the brain tissue between two gyri at 5, 10, and 20 ms. Near boundary Γ_1, all heterogeneous models have lower equivalent stresses compared to the homogeneous model at 20 ms.

In order to obtain a good comparison of the results for all geometries during the complete simulation time,

the maximum and mean equivalent stress from the simulations with loading condition A are shown in Fig. 8 as a function of time. It shows the stresses in the brain tissue only. It can be noticed that the heterogeneous models have a higher maximum equivalent stress than the homogeneous model. Among the heterogeneous configurations, geometry 1 causes a noticeably lower maximum equivalent stress of 112 Pa compared to geometries 2 and 3, with a maximum equivalent stress of approximately 156 Pa. The large maximum equivalent stress in heterogeneous geometry 2 lasts longer than the stresses of the other geometries. The maximum equivalent stress of the homogeneous model reaches a value of 80 Pa. The mean equivalent stresses are nearly the same for all geometries.

To investigate the influence of the heterogeneities, the equivalent stress of the cerebral cortex in the heterogeneous models is taken relative to that of the homogeneous model. For the maximum equivalent stress, this will be done by taking the maximum values, whereas for the mean equivalent stress, this will be done by taking the time averaged values. The maximum equivalent stress of the heterogeneous models 1, 2, and 3 is 1.31, 1.84, and 1.83 times higher than the homogeneous model, respectively. The mean equivalent stress of the heterogeneous models 1, 2, and 3 with respect to the homogeneous model is 1.09, 1.08, and 1.10, respectively.

The equivalent stress fields obtained with loading condition B are displayed in Fig. 9. During the beginning of the simulation, the equivalent stress fields in the brain tissue are comparable for all models. When the field of higher equivalent stress moves downwards, the heterogeneities result in local peak stress concen-
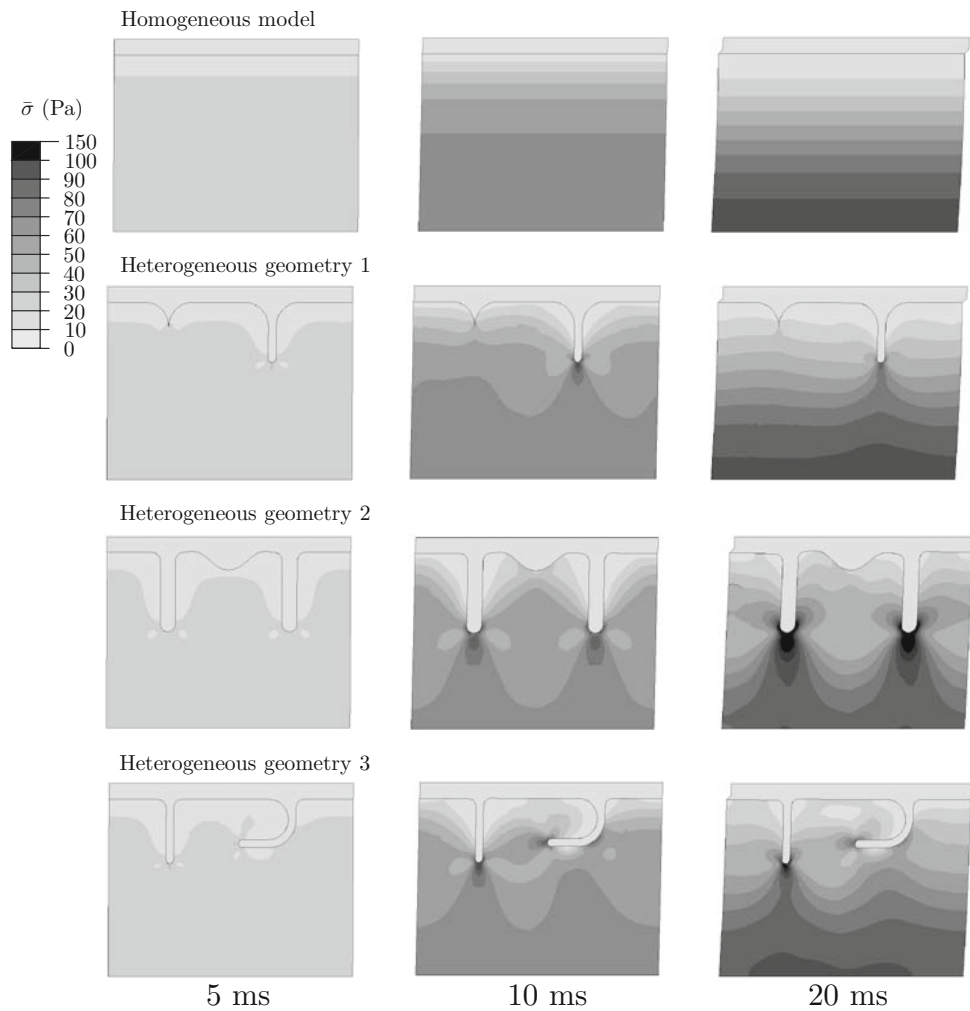
Homogeneous model

$\bar{\sigma}$ (Pa)

150
100
90
80
70
60
50
40
30
20
10
0

Heterogeneous geometry 1

Heterogeneous geometry 2

Heterogeneous geometry 3

5 ms   10 ms   20 ms

FIGURE 7. The equivalent stress fields as a result of loading condition A.

—— Homogeneous, maximum   —— Homogeneous, mean
- - - Geometry 1, maximum   - - - Geometry 1, mean
-·-· Geometry 2, maximum   -·-· Geometry 2, mean
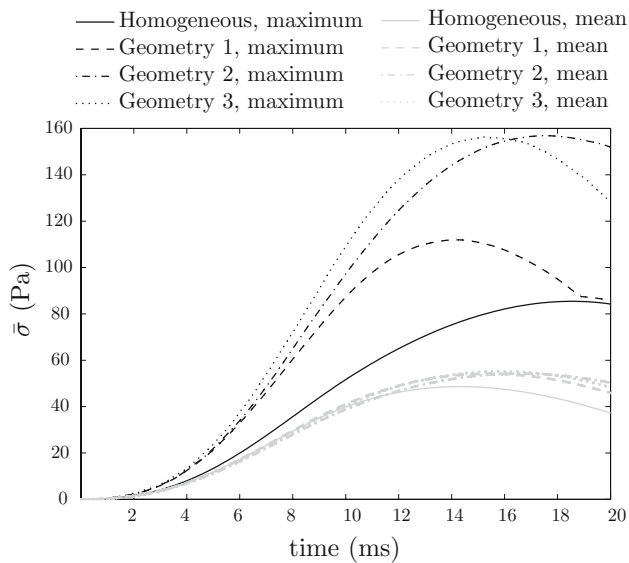······ Geometry 3, maximum   ······ Geometry 3, mean

FIGURE 8. Maximum and mean equivalent stress for the heterogeneous and homogeneous models as a result of loading condition A.

trations, which can be seen at 10 ms for geometries 1 and 3. Later on, at 20 ms, the heterogeneous geometries 1 and 3 have less influence on the equivalent stress fields. The differences of geometry 2 with respect to geometries 1 and 3 are a consequence of the deeper sulci in geometry 2.

The maximum and mean equivalent stress of the cerebral cortex as a function of time obtained with loading condition B is shown in Fig. 10. The maximum equivalent stress is higher for the heterogeneous models than for the homogeneous models, but not for the complete duration of the simulation. After about 10–15 ms, the maximum equivalent stress of the heterogeneous models drops to approximately the same magnitude as the one obtained for the homogeneous model. For the heterogeneous models, the maximum equivalent stress reaches values of approximately 470, 565, and 624 Pa for geometries 1, 2, and 3, respectively. The homogeneous model has a maximum equivalent stress reaching 325 Pa. Also, the moment in
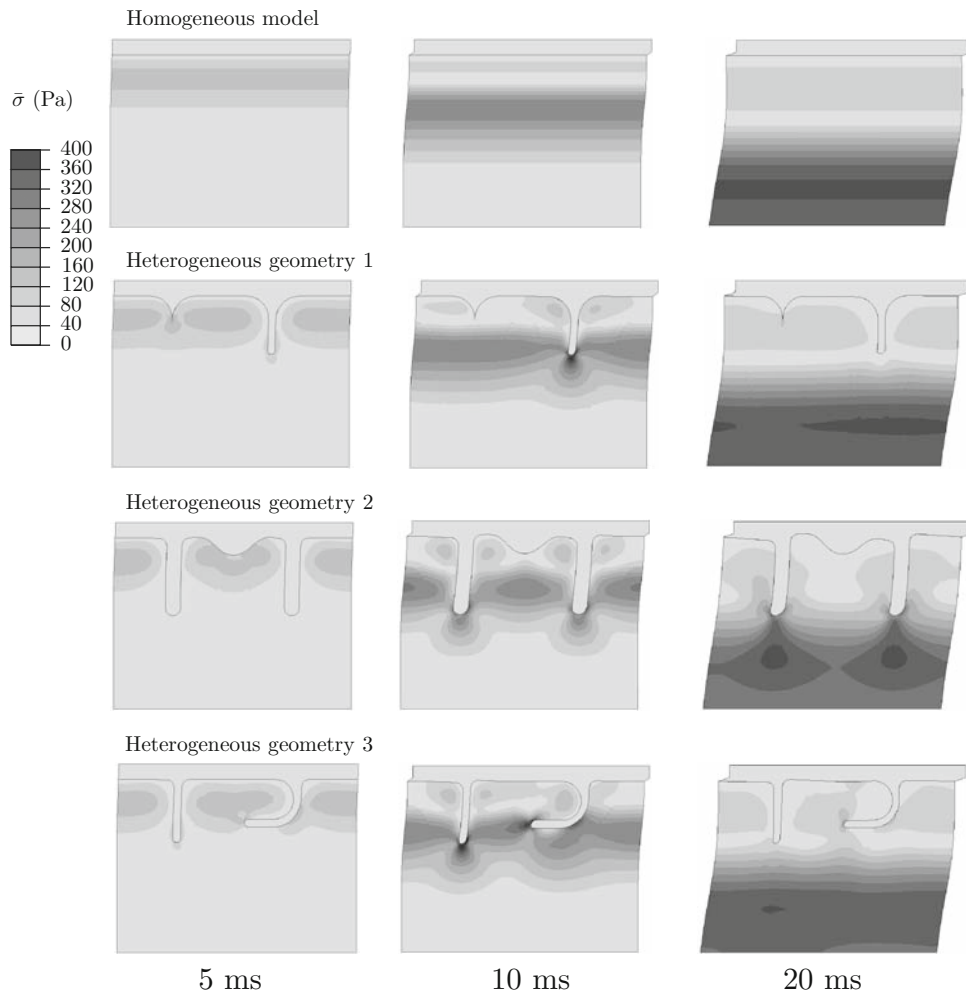
Homogeneous model

$\bar{\sigma}$ (Pa)

400
360
320
280
240
200
160
120
80
40
0

Heterogeneous geometry 1

Heterogeneous geometry 2

Heterogeneous geometry 3

5 ms   10 ms   20 ms

FIGURE 9. The equivalent stress fields as a result of loading condition B.

—— Homogeneous, maximum   —— Homogeneous, mean
- - - Geometry 1, maximum   - - - Geometry 1, mean
-·-· Geometry 2, maximum   -·-· Geometry 2, mean
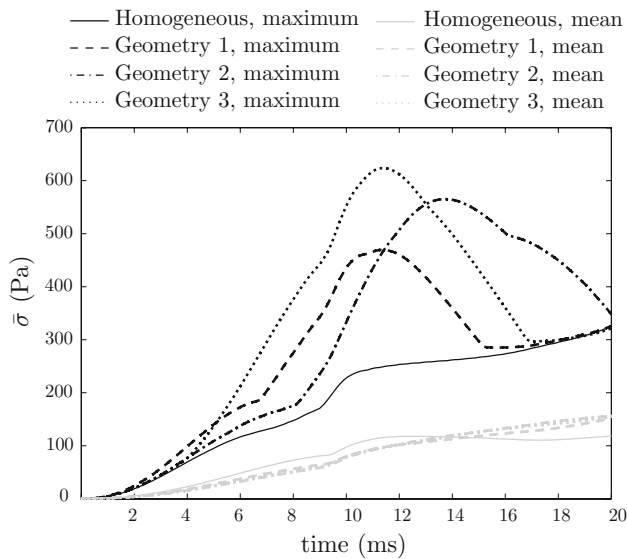······ Geometry 3, maximum   ······ Geometry 3, mean

FIGURE 10. Maximum and mean equivalent stress for the heterogeneous and homogeneous models as a result of loading condition B.

time at which the maximum occurs differs from one geometry to the other. The mean equivalent stress values of all the geometries are similar.

To quantify the influence of the heterogeneities, the equivalent stress of the brain tissue of the heterogeneous models is taken relative to the homogeneous model in the same manner as described previously for loading condition A. The maximum equivalent stress of the heterogeneous models 1, 2, and 3 has increased by 1.44, 1.74, and 1.92 with respect the homogeneous model, respectively. The mean equivalent stress of the heterogeneous models 1, 2, and 3 is 0.97, 0.99, and again 0.99 relative to the homogeneous model, respectively.

The distribution of maximum principal strains for loading condition B at 10 ms is shown in Fig. 11. One can notice that a concentration of maximum principal strains at 10 ms occurs in the same location as the equivalent stress concentration at 10 ms (Fig. 9), both in case of loading condition B. The same method for the quantification of the influence of the heterogeneities is used, but with the maximum principal strain
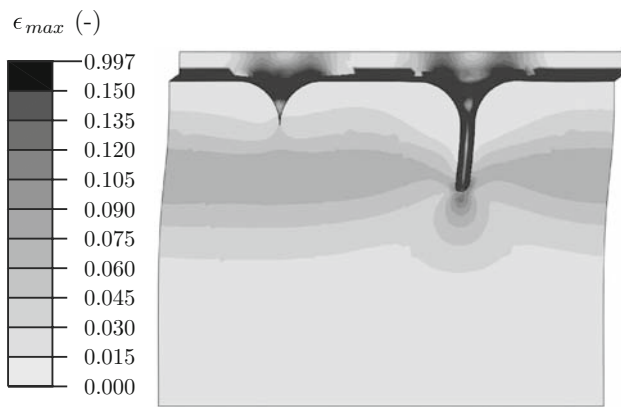
ϵ_{max} (-)

── 0.997
── 0.150
── 0.135
── 0.120
── 0.105
── 0.090
── 0.075
── 0.060
── 0.045
── 0.030
── 0.015
── 0.000

FIGURE 11. The maximum principal logarithmic strain field as a result of loading condition B at 10 ms.

instead of the equivalent stress. For the simulations with loading condition A, the peak maximum principal strain in the brain tissue of the heterogeneous models 1, 2, and 3 has increased with respect to the homogeneous model by 1.22, 1.92, and 1.80, respectively. If loading condition B is used, the increases are 1.43, 1.84, and 1.90, respectively.

DISCUSSION AND CONCLUSIONS

In this study, the influences of the heterogeneities in the cerebral cortex were investigated. This was done with FE models of several different geometries from small detailed parts of the cortex. In a preliminary study, the boundary constraints were tested. The loading conditions were derived from a numerical head model.

In order to determine which constraints on the boundaries would represent the surroundings best, a preliminary study was conducted in which several different constraints were applied to boundaries Γ_1 and Γ_3. The different conditions on boundary Γ_3, i.e., rigid constraint or slip-condition in the x-direction, did not contribute to differences in the results of the brain tissue. This was probably caused by the low shear modulus of the CSF. For boundary Γ_1, several different boundary conditions were tested and compared to the results of models with the same width, but with twice the height of the models in this study. By comparing the 'normal' and the 'high' models, the boundary condition at boundary Γ_1 that represented adjacent brain tissue could be determined. The periodic boundary condition that was applied to boundaries Γ_2 and Γ_4, was used because of the assumed periodicity in the cerebral cortex.

Since the loading conditions were dynamic they could not be applied to the model by directly imposing a deformation, which would induce boundary effects. For this reason, an indirect deformation was imposed by means of body forces. This approach worked well for the first 20 ms of the simulation, which had a total duration of 30 ms. After 20 ms the deformations of the brain tissue differed from the deformations derived from the head model that were indirectly applied to the model (Figs. 6 and 9). Therefore, only the first 20 ms of the simulation are considered to be realistic.

Loading condition A was derived from the acceleration pulse that has been applied to a head model.[6,12] The equivalent stress fields of the homogeneous models caused by loading condition A (Fig. 7) showed no similarities to the equivalent stress field of the head model (Fig. 4). Provided that the equivalent stress field of the head model is realistic, loading condition A can be considered unrealistic. Loading condition B was obtained from the resulting accelerations in the region of interest of the head model. The equivalent stress fields of the homogeneous models from simulations with loading condition B (Fig. 9) were approximately similar to the stress fields in the corresponding region of the head model (Fig. 4) during the first 20 ms. Nevertheless, differences in the equivalent stress fields existed at the surface of the cortex. This is due to the CSF layer in the cerebral cortex model being described elastically with a low shear modulus, as opposed to the head model, which contains a relatively stiff CSF/dura layer. In spite of all these obvious differences, by comparing these two loading conditions, it was shown that the different loading conditions have hardly any effect on the relative mean and maximum equivalent stress and the relative peak maximum principal logarithmic strain. Hence, the mechanical influences of the heterogeneities of the cerebral cortex seem to be independent of the loading conditions.

The constitutive model for brain tissue was based on experiments on porcine white matter.[19] This was used as a substitute for human brain tissue, as it was readily available and it allowed to conduct experiments with a shorter post-mortem time.[12,26] Experiments conducted by Prange *et al.*[37] on fresh human brain tissue indicated that its mechanical properties are approximately 30% stiffer than those of fresh porcine brain tissue. Although the constitutive model for brain tissue in the cerebral cortex model was not based on human brain tissue, the geometries of the models were based on the human cerebrum. This assumption is expected to have more effect on the absolute equivalent stress than on the relative equivalent stress, which is dominated by the heterogeneities of the model. Furthermore, no distinction between the mechanical properties of white and gray matter was made, so that the material properties of the cerebral cortex, which consists of gray matter, were based on experiments on white matter, as

well. In their results, Prange et al.[37] found differences between the material properties of the corpus callosum, i.e., the white matter that connects the two cerebral hemispheres, and the cerebral cortex, but not between the corona radiata, i.e., the white matter that lies inferior to the cerebral cortex, and the cerebral cortex. Nevertheless, in several other studies of head and brain models, different material properties were used for gray and white matter based on the assumption that white matter was more fibrous than gray matter.[2,28,30,47] Therefore, simulations of the cerebral cortex model with shear moduli for gray matter ranging from 75% to 125% with respect to the shear moduli white matter were conducted as well. The results of these simulations indicated that the material properties had an effect on the magnitude of the equivalent stress, but not on the regions in which the peak equivalent stress was observed. The equivalent stress of the heterogeneous model relative to the homogeneous model was hardly affected by the different material properties.

In this model, the meninges and the blood vessels were considered to have no mechanical influence on the cerebral cortex for the used loading conditions. Although Jin et al.[20] suggested that the pia-arachnoid complex can have a mechanical influence on the brain tissue during an impact, it is still not clear if it would affect the influence due to the gyrification of the cerebral cortex. In a study performed by Ho and Kleiven,[17] it was found that the vasculature of the brain can be neglected, as far as the mechanical influences are concerned in a head model not containing the gyrification of the cortex.

In order to validate this model, a comparison with physical experiments is required. However, data of physical experiments at a typical length scale of this level is rather limited. Parallel to this study, the results of physical experiments, in which brain slices have been accelerated, showed increased equivalent strains near the sulci.[24] Furthermore, some studies showed that angular accelerations of the head induce high stress concentrations in and near the cerebral cortex.[8,15] Another method of validation can be performed by comparing the results of the model to clinically observed injury. It has been shown that small cortical infarcts exist in diffuse brain injury at the bottom of the sulci.[40] This is in accordance with the locations of the high stress and strain regions in the cerebral cortex model.

The two loading conditions and the different geometries resulted in different equivalent stress fields. The simulations with loading condition A resulted in a lower mean and maximum equivalent stress compared to the simulations with loading condition B. However, relative to the homogeneous model, it was observed that the equivalent stress was almost independent of the different loading conditions used in this study. The differences between the several heterogeneous geometries had more influence on the relative mean and maximum equivalent stress. The morphologic heterogeneities of the cerebral cortex led to an increase of the maximum equivalent stress by a factor of about 1.3–1.9, depending mostly on the geometry, whereas the relative mean equivalent stress values of all the geometries were 1.1 and 1.0 for loading condition A and B, respectively. Furthermore, the peak maximum principal logarithmic strain was increased by a factor of about 1.2–1.9 due to the morphologic heterogeneities of the cerebral cortex. This is a strong indication that predictions of brain injury obtained from head models with a homogeneous cerebrum should be interpreted with care. To obtain a more accurate assessment of injury, the influence of the morphologic heterogeneities in the cerebral cortex should be accounted for.

ACKNOWLEDGMENTS

OPEN ACCESS

REFERENCES

[1]Acosta, J. A., J. C. Yang, R. J. Winchell, R. K. Simons, D. A. Fortlage, P. Hollingsworth-Fridlund, and D. B. Hoyt. Lethal injuries and time to death in a level I trauma center. *J. Am. Coll. Surg.* 186:528–533, 1998.

[2]Al-Bsharat, A. S., W. N. Hardy, K. H. Yang, T. B. Khalil, S. Tashman, and A. I. King. Brain/skull relative displacement magnitude due to blunt head impact: new experimental data and model. In: Stapp Car Crash Conference Proceedings, Vol. 43, Warrendale, PA: Society of Automotive Engineers, Inc., 1999, pp. 321–332.

[3]Bain, A. C., and D. F. Meaney. Tissue-level thresholds for axonal damage in an experimental model of central nervous system white matter injury. *J. Biomech. Eng.* 122:615–622, 2000.

[4]Bain, A. C., R. Raghupathi, and D. F. Meaney. Dynamic stretch correlates to both morphological abnormalities and

electrophysiological impairment in a model of traumatical axonal injury. *J. Neurotrauma* 18:499–511, 2001.

[5]Bradshaw, D. R. S., J. Ivarsson, C. L. Morfey, and D. C. Viano. Simulation of acute subdural hematoma and diffuse axonal injury in coronal head impact. *J. Biomech.* 34:85–94, 2001.

[6]Brands, D. W. A., P. H. M. Bovendeerd, and J. S. H. M. Wismans. On the potential importance of non-linear viscoelastic material modelling for numerical prediction of brain tissue response: test and application. In: Stapp Car Crash Conference Proceedings, Vol. 46, Warrendale, PA: Society of Automotive Engineers, Inc., 2002, pp. 103–121.

[7]Claessens, M. H. A., A. A. H. J. Sauren, and J. S. H. M. Wismans. Modelling of the human head under impact conditions. In: Stapp Car Crash Conference Proceedings, Vol. 41, Warrendale, PA: Society of Automotive Engineers, Inc., 1997, pp. 315–328.

[8]Cotter, C. S., P. K. Smolarkiewicz, and I. N. Szczyrba. A viscoelastic fluid model for brain injuries. *Int. J. Numer. Methods Fluids* 40:303–311, 2002.

[9]DiMasi, F. P., R. H. Eppinger, and F. A. Bandak. Computational analysis of head impact response under car crash loadings. In: Stapp Car Crash Conference Proceedings, Vol. 39, 1995.

[10]Engel, D. C., J. E. Slemmer, A. S. Vlug, A. I. R. Maas, and J. T. Weber. Combined effects of mechanical and ischemic injury to cortical cells: secondary ischemia increases damage and decreases effects of neuroprotective agents. *Neuropharmacology* 49:985–995, 2005.

[11]Floyd, C. L., F. A. Gorin, and B. G. Lyeth. Mechanical strain injury increases intracellular sodium and reverses Na^+/Ca^{2+} exchange in cortical astrocytes. *Glia* 51:35–46, 2005.

[12]Garo, A., M. Hrapko, J. A. W. van Dommelen, and G. W. M. Peters. Towards a reliable characterisation of the mechanical behaviour of brain tissue: the effects of postmortem time and sample preparation. *Biorheology* 44:51–58, 2007.

[13]Geddes-Klein, D. M., K. B. Schiffman, and D. F. Meaney. Mechanisms and consequences of neuronal stretch injury in vitro differ with the model of trauma. *J Neurotrauma* 23:193–204, 2006.

[14]Goldsmith, W., and K. L. Monson. The state of head injury biomechanics: past, present, and future part 2: physical experimentation. *Crit. Rev. Biomed. Eng.* 33:105–207, 2005.

[15]Gutierrez, E., Y. Huang, K. Haglid, F. Bao, H. Hansson, A. Hamberger, and D. Viano. A new model for diffuse brain injury by rotational acceleration: I. Model, gross appearance, and astrocytosis. *J. Neurotrauma* 18:247–257, 2001.

[16]Henn, H. Crash tests and the head injury criterion. *Teaching Math. Appl.* 17:162–170, 1998.

[17]Ho, J., and S. Kleiven. Dynamic response of the brain with vasculature: a three-dimensional computational study. *J. Biomech.* 40:3006–3012, 2007.

[18]Hrapko, M., H. Gervaise, J. A. W. van Dommelen, G. W. M. Peters, and J. S. H. M. Wismans. Identifying the mechanical behaviour of brain tissue in both shear and compression. In: Proceedings of the IRCOBI Conference, Zurich, Switzerland: IRCOBI, 2007, pp.143–159.

[19]Hrapko, M., J. A. W. van Dommelen, G. W. M. Peters, and J. S. H. M. Wismans. The mechanical behaviour of brain tissue: large strain response and constitutive modelling. *Biorheology* 43:623–636, 2006.

[20]Jin, X., J. B. Lee, L. Y. Leung, L. Zhang, K. H. Yang, and A. I. King. Biomechanical response to the bovine pia-arachnoid complex to tensile loading at varying strain-rates. In: Stapp Car Crash Conference Proceedings, Vol. 50, Warrendale, PA: Society of Automotive Engineers, Inc., 2006, pp. 637–649.

[21]King, A. I. Fundamentals of impact biomechanics: part I – biomechanics of the head, neck, and thorax. *Annu. Rev. Biomed. Eng.* 2:55–81, 2000.

[22]Kleiven, S. Evaluation of head injury criteria using a finite element model validated against experiments on localized brain motion, intracerebral acceleration, and intracranial pressure. *Int. J. Crashworthiness* 11:65–79, 2006.

[23]Kouznetsova, V. G., W. A. M. Brekelmans, and F. P. T. Baaijens. An approach to micro-macro modeling of heterogenous materials. *Comp. Mech.* 27:37–48, 2001.

[24]Lauret, C., M. Hrapko, J. A. W. van Dommelen, G. W. M. Peters, and J. S. H. M. Wismans. An experimental setup for optical characterization of acceleration-induced strain fields in inhomogeneous brain slices (submitted).

[25]Leonov, A. I. Nonequilibrium thermodynamics and rheology of viscoelastic polymer media. *Rheol. Acta* 15:85–98, 1976.

[26]Lind, N. M., A. Moustgaard, J. Jelsing, G. Vajta, P. Cumming, and A. K. Hansen. The use of pigs in neuroscience: modeling brain disorders. *Neurosci. Biohav. Rev.* 31:728–751, 2007.

[27]Mai, J. K., J. Assheuer, and G. Paxinos. Atlas of the Human Brain. 1st ed. London, GB: Academic Press, 1997.

[28]Mao, H., L. Zhang, K. H. Yang, and A. I. King. Application of a finite element model of the brain to study traumatic brain injury mechanisms in the rat. In: Stapp Car Crash Conference Proceedings, Vol. 50, 2006.

[29]Marieb, E. N. Human Anatomy and Physiology. 4th ed. Menlo Park, CA: Benjamin/Cummings Science Publishing, 1998.

[30]Miller, R. T., S. S. Margulies, M. Leoni, M. Nonaka, X. Chen, D. H. Smith, and D. F. Meaney. Finite element modeling approaches for predicting injury in an experimental model of severe diffuse axonal injury. In: Stapp Car Crash Conference Proceedings, Vol. 42, Warrendale, PA: Society of Automotive Engineers, Inc., 1998, pp. 155–167.

[31]Morrison, B., III, H. L. Cater, C. D. Benham, and L. E. Sundstrom. An in vitro model of traumatic brain injury utilising two-dimensional stretch of organotypic hippocampal slice cultures. *J. Neurosci. Methods* 150:192–201, 2006.

[32]Morrison, B., III, H. L. Cater, C. C. Wang, F. C. Thomas, C. T. Hung, G. A. Ateshian, and L. E. Sundstrom. A tissue level tolerance criterion for living brain developed with an in vitro model of traumatic mechanical loading. In: Stapp Car Crash Conference Proceedings, Vol. 47, Warrendale, PA: Society of Automotive Engineers, Inc., 2003, pp. 93–105.

[33]Nishimoto, T., and S. Murakami. Direct impact simulations of diffuse axonal injury by axial head model. *JSAE Rev.* 21:117–123, 2000.

[34]Nolte, J. The Human Brain: An Introduction to its Functional Anatomy. 5th ed. St. Louis, MO: Mosby, Inc., 2002.

[35]Ommaya, A. K., L. Thibault, and F. A. Bandak. Mechanisms of impact head injury. *Int. J. Impact Eng.* 15:535–560, 1994.

[36]Peters, G. W. M., and F. P. T. Baaijens. Modelling of non-isothermal viscoelastic flows. *J. Non-Newtonian Fluid Mech.* 68:205–224, 1997.

[37]Prange, M. T., and S. S. Margulies. Regional, directional, and age-dependent properties of the brain undergoing large deformation. *J. Biomech. Eng.* 124:244–252, 2002.

[38]Raul, J. S., D. Baumgartner, R. Willinger, and B. Ludes. Finite element modelling of human head injuries caused by a fall. *Int. J. Leg. Med.* 120:212–218, 2006.

[39]Shen, F., T. E. Tay, J. Z. Li, S. Nigen, P. V. S. Lee, and H. K. Chan. Modified Bilston nonlinear viscoelastic model for finite element head injury studies. *J. Biomech. Eng.* 125:797–801, 2006.

[40]Strich, S. J. Diffuse degeneration of the cerebral white matter in severe dementia following head injury. *J. Neurol. Neurosurg. Psychiatr.* 19:163–185, 1956.

[41]Tagliaferri, F., C. Compagnone, M. Korsic, F. Servadei, and J. Kraus. A systematic review of brain injury epidemiology in Europe. *Acta Neurochir.* 148:255–268, 2006.

[42]Takhounts, E. G., R. H. Eppinger, J. Q. Campbell, R. E. Tannous, E. D. Power, and L. S. Shook. On the development of the SIMon finite element head model. In: Stapp Car Crash Conference Proceedings, Vol. 47, Warrendale, PA: Society of Automotive Engineers, Inc., 2003, pp. 107–133.

[43]Versace, J. A review of the severity index. In: Stapp Car Crash Conference Proceedings, Vol. 15, Warrendale, PA: Society of Automotive Engineers, Inc., 1971, pp. 771–796.

[44]Welker, W., J. Johnson, and A. Noe. Comparative mammalian brain collections. Technical report, University of Wisconsin, Michigan State and National Museum of Health and Medicine, 2007. www.brainmuseum.org.

[45]Willinger, R., H. Kang, and B. Diaw. Three-dimensional human head finite-element model validation against two experimental impacts. *Ann. Biomed. Eng.* 27:403–410, 1999.

[46]Wood, J. K. Dynamic response of human cranial bone. *J. Biomech.* 4:1–12, 1971.

[47]Zhou, C., T. B. Khalil, and A. I. King. A new model comparing impact responses of homogeneous and inhomogeneous human brain. In: Stapp Car Crash Conference Proceedings, Vol. 39, Warrendale, PA: Society of Automotive Engineers, Inc., 1995, pp. 121–137.